Heliyon 10 (2024) e32808

Contents lists available at ScienceDirect

Heliyon

journal homepage: www.cell.com/heliyon

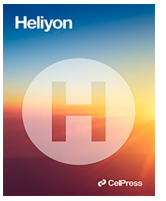

Research article

# Development of 3D skin equivalents for application in photodynamic biostimulation therapy assays using curcumin nanocapsules

Camila F. Amantino [a,**], Stéphanie R. do Amaral [a], Mariza Aires-Fernandes [a], Sonia M. Oliani [c], Antonio C. Tedesco [b], Fernando L. Primo [a,*]

[a] *Department of Bioprocess Engineering and Biotechnology, São Paulo State University (UNESP), School of Pharmaceutical Sciences, Araraquara, São Paulo, 14800-903, Brazil*

[b] *Department of Chemistry, Center of Nanotechnology and Tissue Engineering – Photobiology and Photomedicine Research Group, Faculty of Philosophy, Sciences and Letters of Ribeirão Preto, University of São Paulo - USP, Ribeirão Preto, São Paulo, 14010-100, Brazil*

[c] *Department of Biology, Institute of Biosciences, Languages and Exact Sciences (IBILCE), São Paulo State University (UNESP), São José do Rio Preto, SP, 15054-000, Brazil*

ARTICLE INFO

*Keywords:*
Tissue engineering
Three-dimensional skin equivalents
Photodynamic biostimulation therapy
Curcumin
Nanocapsules

ABSTRACT

For decades, animal models have been the standard approach in drug research and development, as they are required by regulations in the transition from preclinical to clinical trials. However, there is growing ethical and scientific concern regarding these trials, as 80 % of the therapeutic potential observed in pre-clinical studies are often unable to be replicated, despite demonstrating efficacy and safety. In response to this, Tissue Engineering has emerged as a promising alternative that enables the treatment of various diseases through the production of biological models for advanced biological assays or through the direct development of tissue repairs or replacements. One of the promising applications of Tissue Engineering is the development of three-dimensional (3D) models for in vitro tests, replacing the need for in vivo animal models. In this study, 3D skin equivalents (TSE) were produced and used as an in vitro model to test photobiostimulation using curcumin-loaded nanocapsules. Photodynamic biostimulation therapy uses photodynamic processes to generate small amounts of reactive oxygen species (ROS), which can activate important biological effects such as cell differentiation, modulation of inflammatory processes and contribution to cell regeneration. The PLGA nanocapsules (NC) used in the study were synthesized through a preformed polymer deposition method, exhibiting particle size <200 nm, Zeta potential >|30| and polydispersity index between 0.5 and 0.3. Atomic force microscopy analyzes confirmed that the particle size was <200 nm, with a spherical morphology and a predominantly smooth and uniform surface. The NC biocompatibility assay did not demonstrate cytotoxicity for the concentrations tested (2.5–25 μg $mL^{-1}$).The in vitro release assay showed a slow and sustained release characteristic of the nanocapsules, and cellular uptake assays indicated a significant increase in cellular internalization of the curcumin-loaded nanostructure. Monolayer photobiostimulation studies revealed an increase in cell viability of the HDFn cell line (viability 134 %–228 %) for all LED fluences employed at λ = 450 nm (150, 300, and 450 mJ $cm^{-2}$). Additionally, the scratch assays, monitoring in vitro scar injury, demonstrated more effective effects on cell

* Corresponding author.
** Corresponding author.
*E-mail addresses:* camila.amantino@unesp.br (C.F. Amantino), fernando.primo@unesp.br (F.L. Primo).

https://doi.org/10.1016/j.heliyon.2024.e32808
Received 12 December 2023; Received in revised form 7 June 2024; Accepted 10 June 2024
Available online 11 June 2024

proliferation with the fluence of 300 mJ $cm^{-2}$. Staining of TSE with hematoxylin and eosin showed the presence of cells with different morphologies, confirming the presence of fibroblasts and keratinocytes. Immunohistochemistry using KI-67 revealed the presence of proliferating cells in TSE after irradiation with LED $\lambda = 450$ nm (150, 300, and 450 mJ $cm^{-2}$).

## 1. Introduction

Tissue Engineering (TE) is one of the most important areas of research in present times, as it unites the principles of engineering and life sciences for the further development of biomaterials that are alternatives to biological systems and substitutes that can improve and restore tissue functions [1,2]. The principle of TE is incorporating cells into support to reproduce the three-dimensional structure of tissues, which can also restore the tissue's physical, mechanical, and biological properties [3]. In the field of skin, TE has been used to develop skin substitutes that reproduce human skin. They are called equivalents or three-dimensional skin models used for implants and lesion repair [4,5].

Three-dimensional Skin Equivalents (TSE) are cellular culture matrices that reproduce skin functions and in vivo morphology. In addition to their use as substitutes for conventional grafts. TSEs have been used in testing new drugs and screening compounds to reduce the use of animals in research [6,7]. The proposal to develop a TSE arose from the possibility of culturing fibroblasts and keratinocytes in vitro, together with matrices that make up the skin. The first protocols date from the 70′s and use monocultures of keratinocytes or fibroblasts with a collagen-like matrix. Currently, the seeding of cell co-culture has been studied to produce a complete epidermis [8]. TSE can be used as human skin equivalent models in scientific and technological areas. In addition to their role as a substitute in the treatment of lesions. These models are important tools in studying skin-related diseases and injuries [8,9]. With the growing desire to reduce the use of animals in research, the search for alternatives is of great importance [6,10]. In this context, the use of TSEs for the development of 3D skin equivalents capable of mimicking tissue functions for safety and strength tests has shown to be a very promising area [11].

Photodynamic therapy (PDT) is a therapeutic modality that has been widely studied for the treatment of cancer and skin diseases, conventional treatments are mostly a combination of surgical interventions and pharmacological treatment, leading to severe side effects, such as hair loss. , nausea and weight loss, as is the case with chemotherapy, in addition, many of these therapies require the excessive use of antibiotics, which leads to yet another global concern, bacterial resistance [12–14]. Therefore, PDT presents itself as a less invasive alternative and, therefore, has great acceptance among patients and has proven to be very efficient due to its selectivity, versatility and therapeutic simplicity [15,16]. PDT has been widely studied for its application in treating several diseases featuring certain types of cancer. Its mechanism consists of the use of three components, a molecule capable of absorbing monochromatic energy at a specific wavelength, a compound called a photosensitizer (PS), an energy source (LASER or LED), and also molecular oxygen present in a microenvironment like our body [17,18]. The combination of these components leads to specific reactions and results in the production of highly reactive singlet oxygen and other reactive derivative oxygen species, which when in contact with specific targets can lead to death [15].

In this framework the Photobiomodulation therapy (PBT) or laser therapy consists of using low-intensity light sources to activate endogenous chromophores to generate cell regeneration activation and anti-inflammatory responses [2,19,20]. Studies demonstrate the benefits of this therapy, such as increased post-traumatic neuronal function, stimulation of neuronal growth, protective effects on post-ischemia cardiomyocytes, modulation of the immune system, bone tissue remodeling and repair, and nerve and muscle regeneration [2,2,21,21,22,22,23,23,24,24,25,25]. Studies also demonstrate effects of PBT on collagen production, fibroblast proliferation, extracellular matrix and reduced inflammatory response, and metalloprotease regulation, making it an alternative therapy for healing and tissue repair processes [26].

Although the initial objective of PDT is the production of high concentrations of ROS, which leads to cell damage, resulting in apoptosis and/or necrosis of pathogenic cells [27], studies indicate that the decrease in the density of excitation energy and consequently a low ROS production can lead to a biostimulator response in cells, tissues or organs, similar to what already happens with PBT, activating metabolic ways, with cell growth, differentiation and regeneration responses [28,29].

Photosensitizer are chemical compounds classified as dyes (natural or synthetic) capable of absorbing light at a specific wavelength and then triggering a series of photochemical reactions resulting in the production of $^1O_2$ and ROS [30]. In this context, curcumin is a natural compound that holds significant potential as a photosensitizer [31].Moreover, it has garnered considerable medicinal interest based on preliminary studies, showing its potential for the treatment and prevention of various pathologies, such as inflammatory, cardiovascular, neurodegenerative, and neoplastic diseases, while also exhibiting strong antioxidant action [32,33] The therapeutic versatility of curcumin stems from its broad regulatory capacity over molecular targets, including growth factors, transcription factors, cytokine receptors, enzymes, and genes responsible for cell proliferation and apoptosis [31].

The effectiveness of curcumin in in vitro and in vivo systems is directly related to its bioavailability, which is a problem, as its solubility in aqueous media is low and when in aqueous media, its inactivation occurs, in addition to having membrane permeability. Limited [34]. Therefore, several studies demonstrate the need to combine curcumin with pharmaceutical nanotechnology, that is, using a nanocarrier to protect and improve its bioavailability [35–37]. The development of nanocarriers containing these PS, aims to promote advantages, such as better solubility in biological media, as well as presenting reduced particle size, which provides passive accumulation in target tissues and reduces the concentration of PS needed for a therapeutic response similar to the free form of the PS [37]. In addition, nanocarrier systems offer more efficient drug transport, and the nanometric size promotes a passive accumulation

effect in pathogenic tissues. In addition, it has biocompatibility, which promotes a controlled and sustained release, reduces adverse effects inherent to the drug, and expands forms of administration [38]. Previous studies have demonstrated the release profile of curcumin associated with nanoparticles, indicating a controlled and sustained release over a long period of time [35,39].

Polymeric-coated nanoemulsions or polymeric nanocapsules (NC) stand out among nanocarriers. Their advantages range from their prolonged stability, low cost of obtaining and their ability to promote a controlled release. It is also possible to observe their ability to encapsulate actives with distinct solubility, making them biocompatible and biodegradable [40–42].

In this context, our work developed a 3D skin equivalent as an alternative to animal use in trials, to evaluate the proliferative effect of applying polymeric nanocapsules with curcumin photodynamic biostimulation therapy (PDBT). At the same time, polymeric nanocapsules with curcumin were developed and characterized for use in cell proliferation PDBT assays.

## 2. Materials and methods

Acetone, Phospholipids (soy phosphatidylcholine), Soy Oil, PLGA copolymer, Curcumin, Kolliphor P188 (non-ionic surfactant), Dulbecco's Modified Eagle's Medium (DMEM), Fetal bovine serum (FBS), Ampicillin/streptomycin, HDFn ATCC® PCS-201-010™, HaCat-Cell Lines Service, NIH/3T3 ATCC® CRL-1658™, EnSpire® microplate reader (PerkinElmer, USA), Resazurin solution, Microplate reader EnSpire® (PerkinElmer, USA), Table LED (IrradLED/Biopdi, São Carlos, SP, Brazil), Hematoxylin, Eosin, Ki-67 antibody (Abcam ab16667), 4 % paraformaldehyde, PBS buffer, Glycine, Triton X-100, DAPI (4′,6-diamidino-2-phenylindole),TCS-SP8 confocal laser microscopy (Leica Microsystems).

### 2.1. Synthesis of curcumin nanocapsules

The curcumin nanocapsules (Curc/NC) were prepared according to a nanoprecipitation or interfacial deposition of the preformed polymer method described by Fessi 1989 [43] with modifications by Siqueira-Moura 2013 [27]. This method is responsible for the spontaneous formation of nanometric oil droplets with polymeric membrane coating. Briefly, the organic phase using acetone was prepared containing phospholipids (soy phosphatidylcholine 1.75 %), oil (1.67 %), PLGA copolymer(0.75 %) and curcumin (Curc) at 40 °C. Subsequently, this solution was added to the aqueous phase containing Kolliphor P188 (1.25 %) as a non-ionic surfactant. The organic solvent was completely removed by rotary-evaporation under reduced pressure at 40 °C.

### 2.2. Particle size, zeta potential and physical-chemical stability

The particle size, PdI, and Zeta potential, were measured using the particle analyzer Zetasizer, Nano ZS90 Malvern model, operating at 633 nm and adjusted to detect a scattering angle of 90°.

### 2.3. Accelerated stability

The stability of the Curc/NC and Unload/NC dispersions was analyzed using a dispersion analyzer called the LUMiSizer 611, manufactured by LUM GmbH in Berlin, Germany. The analyzer employed STEP Technology (Space and Time resolved Extinction Profiles) to conduct the study. This technology allowed for the simultaneous registration of transmitted light intensity (at 880 nm) as a function of both time and position over the sample. The measurements were conducted at a constant temperature of 25 °C. The transmission profile was recorded every 65 s over a period of 476 min, with the rotation speed set at 3618 rpm. To perform the analyses, specific cuvettes with a radius position of 129.5 mm were utilized.

### 2.4. Atomic force microscopy

The atomic force microscopy (AFM) is able to scan high-resolution tridimensional images of the topographic surface of the analyzed material. Images were obtained using the tapping mode technique performed with a Scanning Probe Microscope SPM-9600 (Shimadzu, Kyoto, Japan) controlled by SPM Online software. A droplet of the NC and Curc/NC samples were deposited on a freshly cleaved mica surface and naturally dried. The images were acquired using the tapping mode technique, with a silicon cantilever 124 μm in length. The resonance frequencies ranged from 324 to 369 kHz, and the spring constants varied from 34 to 51 N $m^{-1}$.

### 2.5. Cell culture human fibroblasts HDFn and keratinocytes HaCat

We used Primary Normal Human Dermal Fibroblasts, Neonatal (HDFn ATCC® PCS-201-010™), Keratinocytes (HaCat-Cell Lines Service), and a commercial fibroblast cell line obtained from a mouse NIH/Swiss embryo (NIH/3T3 ATCC® CRL-1658™). Cells were grown in Dulbecco's Modified Eagle's Medium (DMEM) supplemented with 10 % fetal bovine serum (FBS) (Gibco, New York, USA) and 20 μg $mL^{-1}$ ampicillin/streptomycin (USB Corporation). Cultures were maintained at 37 °C in a humidified atmosphere of 5 % $CO_2$. Upon reaching total confluence, these cells were utilized as biological models for cytotoxicity and photomodulation studies.

### 2.6. Uptake cells study

The cell uptake assay was performed using the commercial cell lines HDFn ATCC® PCS-201-010™, HaCat-Cell Lines Service, and

NIH/3T3 ATCC® CRL-1658™. The cells were cultivated following the protocol in section 2.5 until reaching confluence. Cells were seeded into 24 wells at a density of $3 \times 10^4$ cells/well. Curcumin-loaded nanocapsules (Curc/NC) were used for the test at concentrations of 5 and 25 μg $mL^{-1}$. The incubation times were 3, 6, and 24 h. After the incubation, the cells were washed with 1x PBS to remove Curc and Curc/NC that were not taken up by the cells. Finally, fluorescence analysis was performed using an EnSpire® microplate reader (PerkinElmer, USA) with excitation wavelength at 415 nm and emission at 540 nm.

### 2.7. Cytotoxicity assay using resazurin test

NIH/3T3 ATCC® CRL-1658™ cell line was seeded into a 96-well plate (5 × 103 cells/well). After 24 h Unloaded/NC and Curc/NC were added at a concentration range of 2.5–25 μg $mL^{-1}$ using mean DMEM for dilutions and incubated for 3 h. After 24 h of treatment, 20 μL of Resazurin solution (25 μg $mL^{-1}$ in PBS) and 180 mL of DMEM phenol-red free were added and incubated for 4 h. Afterwards, the wells analyses were carried out in the microplate reader EnSpire® (PerkinElmer, USA) in 570 nm and the basal absorbance was corrected in 590 nm. The percentage of viable cells was calculated following Equation (1).

$$\text{viable cells } (\%) = (\text{O.D.sample} \ / \ \text{O.D.control}) \times 100 \quad (1)$$

### 2.8. Photobiostimulation in monolayer monitoring cell proliferation using colorimetric method with resazurin after irradiation

The Hacat and HdFn cell lines were cultivated according to the protocol described in section 2.5 until they reached confluence. Then, they were plated in 24-well plates and incubated for 24 h. After which time the plates were incubated with Curc/NC at a concentration of 5.0 μg $mL^{-1}$ for 3 h and a control containing only culture medium. After incubation the cells were washed with 1x PBS and culture medium without phenol red was added. Then, irradiation was carried out using a table LED as the light source (IrradLED/Biopdi, São Carlos, SP, Brazil) with energy doses of 150, 300 and 450 mJ $cm^{-2}$. In the sequence, 48 h after the irradiation, the colorimetric method with resazurin described in the section was used to assess cell proliferation after photobiostimulation.

### 2.9. Photobiostimulation in monolayer culture: evaluation of cell migration after induction of cicatricial lesion in vitro

For the cell migration assay, the protocol described by Premarathna et al. [44], was used with modifications. Hacat and HdFn cell lines were cultured according to the protocol described in section 2.5 until reaching the confluence. Then, they were plated in 24-well plates and incubated until they reached 100 % confluence. Once cell confluence was reached, a groove was made with the help of a tip of 1000 μL sterile plastic (pipette tip width approximately 800 μm) that was gently pulled across the coverslip surface in all wells. After slotting the plates were incubated with Curc/NC at a concentration of 5.0 μg $mL^{-1}$ for 3 h and a control containing only culture medium. After incubation the cells were washed with 1x PBS and culture medium without phenol red was added. Then, irradiation was performed using the LED table (IrradLED/Biopdi, São Carlos, SP, Brazil) with energy doses of 150, 300 and 450 mJ $cm^{-2}$. A microscope calibration ruler and photomicrographs were used to monitor the closure of the slots as a function of time (0; 1 h; 6 h; 24 h; 48 h).

### 2.10. Preparation of three-dimensional skin equivalents (TSE)

TSEs were prepared from dermal equivalents (DE) following the protocol described by Ref. [45] with an improvement for the production of three-dimensional skin equivalents (TSE) based on the protocols described by Ref. [46]. In summary, initially the fibroblasts and type I collagen are mixed and added to a Petri dish for the formation of the ED. After 4 days of preparation, the EDs were transferred to 6-well plates and HaCat cells were added to the EDs at a density of $2 \times 10^5$ cells/ED and incubated for 1 h. Thereafter, the culture medium containing Hacat was removed and DMEM with 10 % FBS was added. The medium was replaced with fresh medium every other day. The effects of the formation of the three-dimensional network and tissue layers of the TSE were monitored by high-resolution microscopy.

### 2.11. Hematoxylin and eosin (HE) stain

The samples were stained with hematoxylin and eosin (HE) intercalated with water and applied to star frost slides to evaluate cell morphology. Histological images were captured with an optic microscopy.

### 2.12. Immunohistochemistry

Immunostaining was performed 24 h after the irradiation, using the Ki-67 antibody as a marker (Abcam ab16667). TSEs were washed twice with PBS (1x) and fixed with 4 % paraformaldehyde diluted in PBS buffer (1x) for 20 min on ice. Subsequently, the TSEs were washed 2 times with PBS (1x) containing 100 mmol $L^{-1}$ glycine (Sigma) and permeabilized with 0.1 % Triton X-100 (Sigma) diluted in PBS (1x) for 10 min at room temperature. The TSEs were then washed twice with PBS (1x). Soon after, the TSEs were incubated with the primary antibody, Ki-67 (Abcam) (diluted 1:5 in blocking solution) for 3 h, in a humid chamber, at room temperature. TSEs were washed 2 times with PBS (1x). Subsequently, samples were incubated with the secondary antibody (DAPI (4′,6-diamidino-2-phenylindole) for 1.5 h at room temperature. Slides were observed in TCS-SP8 confocal laser microscopy (Leica Microsystems). DAPI and Ki-67 were detected at excitation/emission 405/461 nm and 638/650 nm respectively.

### 2.13. Statistical analysis

The results of experiments from sessions 3.4, 3.5 and 3.6 were performed in triplicate and expressed as mean ± standard deviation (SD). Data from the treated groups were compared to the respective negative control experiments. Statistical analyzes were performed using one-way analysis of variance (one-way ANOVA). Significant comparisons between groups were performed using Tukey's *t*-test and post-test for multiple comparisons (*$p < 0.05$).

## 3. Results

### 3.1. Particle size, zeta potential and physical-chemical stability

The dynamic light scattering (DLS) technique was used to determine size distributions, polydispersity index, and electrophoretic measurement. All analyses were carried out on unload/NC and Curc/NC samples. Table 1 presents the results expressed as mean ± standard deviation. The unloaded NC and Curc/NC results showed adequate particle size <250 nm (from 130.58 ± 30.3 nm to 106.3 ± 48.4 nm) and high values for Zeta potential (from −45.0 mV to −43.5 mV) were observed. The polydispersity index values (0.78 and 0.46, respectively) denote the tendency of the polydisperse system, however, this was only 97 days after synthesis.

### 3.2. Accelerated stability

The evaluation of nanomaterials plays a crucial role in optimizing their properties and applications. LUMiSizer® is a monitoring tool used to assess the separation performance of colloidal dispersions. It employs centrifugal separation analysis to record transmission profiles, which represent the variation of transmitted light over time and space during the separation process. By analyzing these profiles, valuable information about the kinetics of the separation process is obtained. Specifically, the migration speed of particles can be calculated, and this parameter is directly linked to the particle size distribution. Consequently, it becomes possible to estimate the stability of nanocrystals (NCs) based on these data [41,47,48]. In Fig. 1, the transmission profiles of two samples are shown: Curc/NC and Unloaded/NC samples.

The LUMiSizer® also provides quantitative instability index data. This parameter is calculated based on the increase in transmission when there is phase separation by the sedimentation or creaming processes in each separation time, divided by the maximum clarification. Table 2 presents the obtained indexes, which is a dimensionless number, ranging from 0 (mostly stable) to 1 (mostly unstable), and Fig. 1 (A,B) show the transmission profile of the Curc/NC and Unloaded/NC [48].

### 3.3. Atomic force microscopy

The three-dimensional AFM topographic analysis of Curc/NC (Fig. 2A) and Unloaded/NC (Fig. 2B) showed clear images of the spherical particles. The results also demonstrate a morphology with an absence of roughness on the surface and a tendency of drug interaction within the particles. From the topographic profile, it was possible to measure the average particle size of 126 nm for Curc/NC and 144 nm for Unloaded/NC. These values are near to DLS data previously obtained for hydrodynamic analyses.

### 3.4. Uptake cellular assays

Cellular uptake studies are essential to understand the potential biodistribution and intracellular delivery of therapeutic agents, as well as to evaluate the safety and efficacy of new drug delivery systems. Cellular uptake studies were performed using the three cell lines (NIH-3T3, HdFn, and HaCat), the results are shown in Fig. 3A,B,C.

### 3.5. Cytotoxicity assay using resazurin test

Cell viability and cytotoxicity studies of nanomaterials and new compounds are important for future clinical applications. Fig. 4 shows ≥100 % cell viability results, which confirm the absence of cytotoxicity for all tested concentrations of Curc/NC, including Unloaded/NC 50 % (v/v). From these results, the concentration of 5 μg $mL^{-1}$ of Curc/NC was chosen for the Photobiostimulation assay.

### 3.6. Photobiostimulation in monolayer monitoring cell proliferation using colorimetric method with resazurin after irradiation

The monolayer photobiostimulation study was performed using commercial cell lines of human neonatal HDFn dermal fibroblasts

**Table 1**
Data of particle size, PDI, and zeta potential of NC formulations.

| Zeta Potential (mV) | PdI | Particle size (nm) | Sample |
|---|---|---|---|
| −45.0 ± 4.7 | 0.78 ± 0.3 | 130.6 ± 30.3 | Unloaded NC |
| −43.5 ± 5.4 | 0.46 ± 0.1 | 106.3 ± 48.4 | Curc/NC |

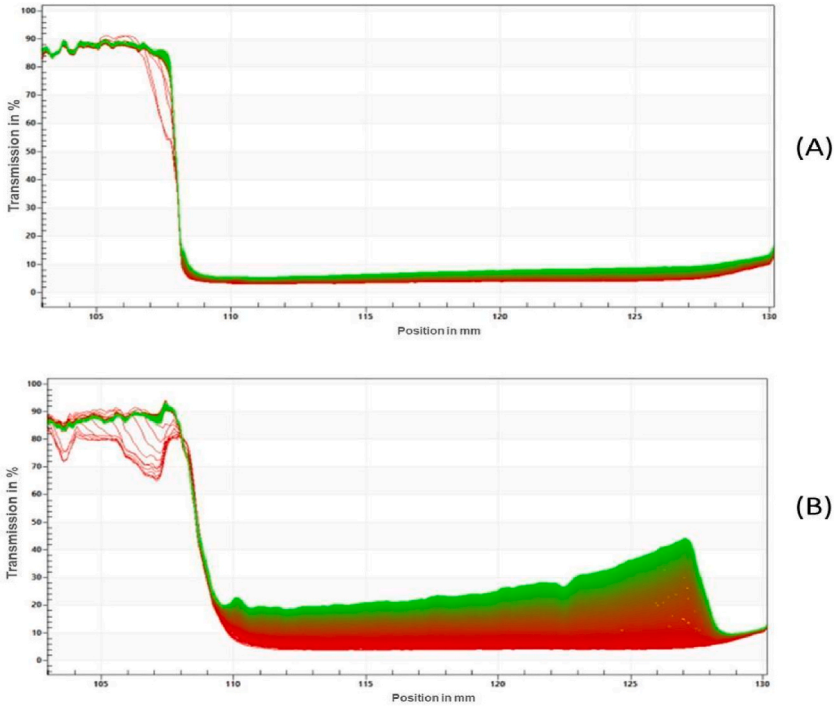


**Fig. 1.** Transmission profiles obtained with Curc/NC (A) and unloaded/NC samples (B) by forced stability analysis during analytical centrifugation. The first and the last registered profiles are shown in red and in green, respectively. (For interpretation of the references to color in this figure legend, the reader is referred to the Web version of this article.)

**Table 2**
Instability index of Curc/NC and Unloaded/NC, measured after production stored at 25 °C.

| Instability Index | Storage Temperature [°C] | Scheme. |
|---|---|---|
| 0.042 | 25 | Curc/NC |
| 0.240 | 25 | Unloaded/NC |

to find a protocol for future studies in TSE. In the studies we used 150, 300 and 450 mJ $cm^{-1}$ and Curc/NC at a concentration of 5.0 μg $mL^{-1}$ was used. Fig. 5 shows the representation of the data obtained 48 h after irradiation.

### *3.7. Photobiostimulation in monolayer monitoring: evaluation of cellular migration after induction of in vitro cicatricial lesion*

For monolayer photobiostimulation studies evaluating cell migration after induction of scar lesion, we used HaCaT human keratinocyte lines, LED doses of 150, 300 and 450 mJ $cm^{-1}$, and Curc/NC at a concentration of 5.0 μg $mL^{-1}$ (incubated for 3 h). Images of monitoring were performed as shown in the micrographs below (Fig. 6). The mimetic lesion closure (scratch) measurement was performed with a microsection ruler to monitor the kinetics of groove closure.

### *3.8. Three-dimensional skin equivalents (TSE) in vitro*

To obtain the DE the fibroblast was used in addition to collagen type-I solution, and the 3D matrix construction was used to obtain the DEn. Collagen is the main functional and structural protein present in the extracellular matrix of the human dermis. Among natural materials, collagen is the most used for clinical studies for developing Tissue Engineering. This is because collagen has low immunogenicity and biocompatibility, which means that its use is safe and effective in the production of DEs. In addition, the pores formed in their structures provide a microenvironment that favors cell adhesion, migration, and proliferation in protocols that allow co-culture [49–51]. After 4 days of DE development (Fig. 7A), keratinocytes were added to form the TSE (Fig. 7B and D). Fig. 7B shows the TSE after 4 days of its preparation, we can observe the formation of the keratinocyte layer.

### *3.9. Immunohistochemistry*

Hematoxylin and eosin were used to stain the presence of cells in TSE and to show the morphological difference between

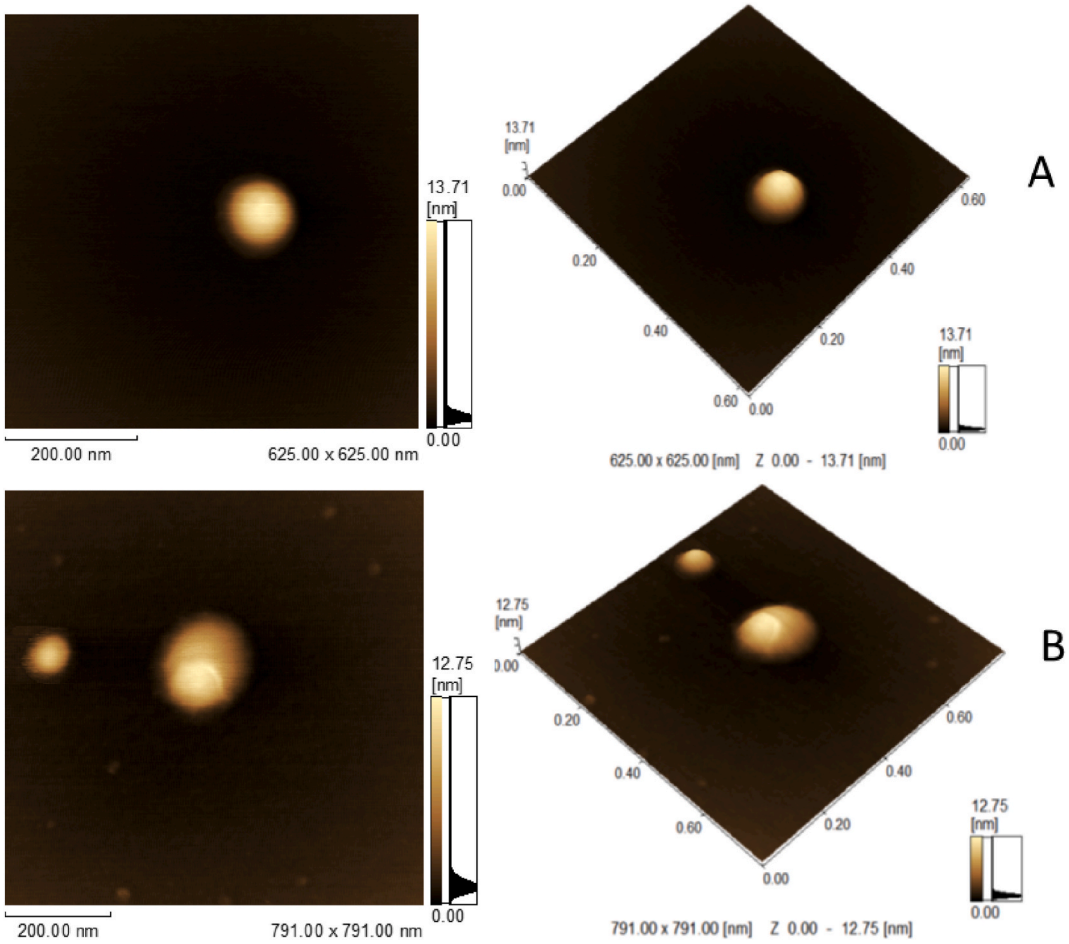


**Fig. 2.** Two and Three - dimensional photomicrography of topographic morphology profile of Curc/NC (A) and Unloaded/NC (B).

keratinocyte and fibroblast cell lines (Fig. 7C).

The Ki-67 antibody is widely used to label proliferating cell nuclei in healthy and tumor cell populations to measure cell proliferation in the TSE 12 days after its preparation and 24 h after irradiation. DAPI was also used for nuclear labeling (Fig. 8)

Using the ImageJ software, it was possible to obtain quantitative data to compare the expression of Ki-67 between the TSE incubated with Curc/NC and its control at different doses of energy. The data were statistically analyzed, and the result is shown in Fig. 9.

## 4. Discussion

Obtaining reliable data so nanoparticles can be properly characterized is extremely important, as the behavior of nanomaterials in a biological environment is directly related to their physicochemical properties [52,53]. Dissolution, toxicity, and cellular uptake are some of the many biological effects for which nanomaterials' particle size and surface charge (Zeta potential) are responsible. Together with the polydispersity index (PDI), they are used to monitor the stability of colloidal nanomaterials [53]. The particle size $\leq$250 nm, allows for routes of administration to be expanded, and promotes the effect of passive accumulation in injured tissues. In this way we can have a selectivity for treating various diseases. The PdI is an index that characterizes how homogeneous and dispersed the suspended particles are. The index $\leq$0.3 ensures that the formation of agglomerates, and consequent changes in particle size, occur less frequently [54].

The results show the average particle size within the defined size (<250 nm) for both Curc/NC and NC/Empty. However, this was not found below the index corresponding to 0.3. This is because a small population of particles with sizes between 300 nm–2000 nm are present in the Curc/NC and NC/Empty formulations, which causes the PdI to be between 0.5 and 1, well above the defined standards. However, in both formulations, physicochemical characteristics for both samples (Curc/NC and NC/unloaded) were observed during the 97-day follow-up, showing particle size in size dimensions (<200 nm) to more than 90 % of the particles present in the formulation. The Zeta potential is within the target profile of $\geq$ |-30| mV, which represents a surface with predominantly negative residual charge, a common characteristic of nanomaterials obtained with coatings of copolymers of the polyoxypropylene class and

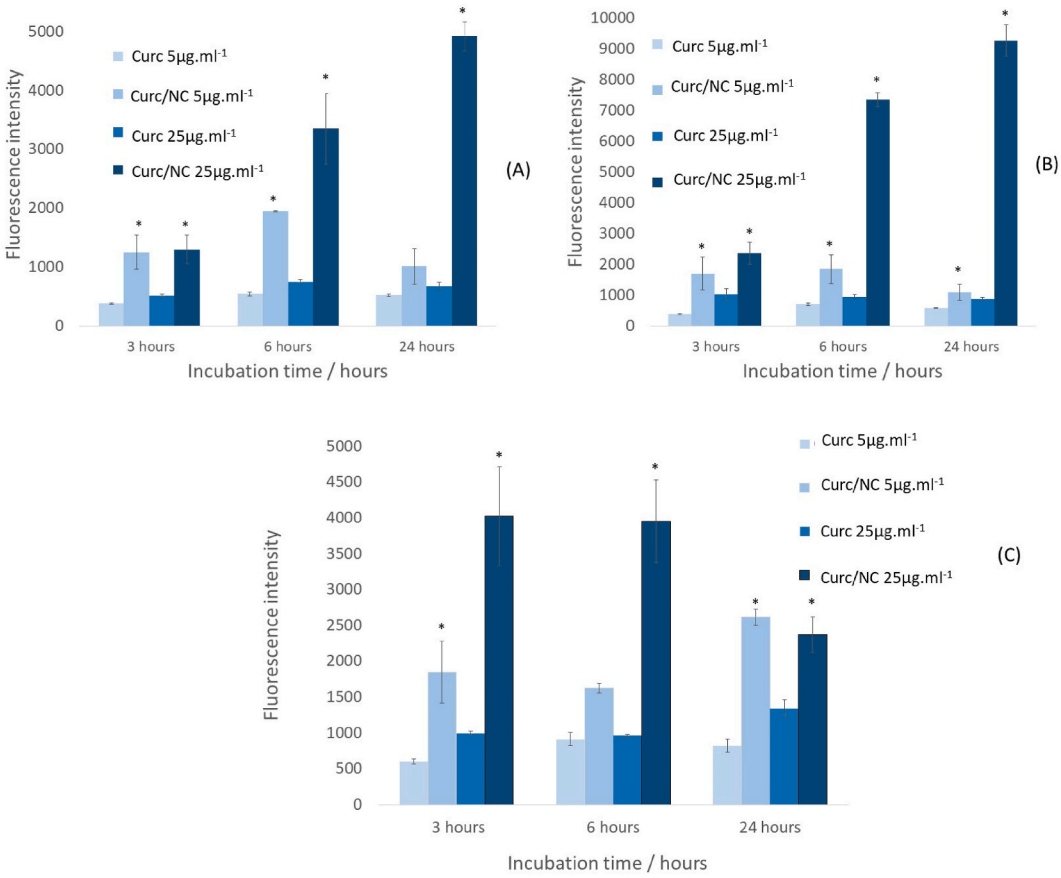


**Fig. 3.** Cell uptake study using NiH-3T3 (A), HdFn (B) and HaCat (C) cell lines (mean and standard deviation) Statistical significance was determined by the One-way ANOVA analysis of variance test followed by the Tukey post-test *t*-test for multiple comparisons (*p < 0.05) for n = 3.

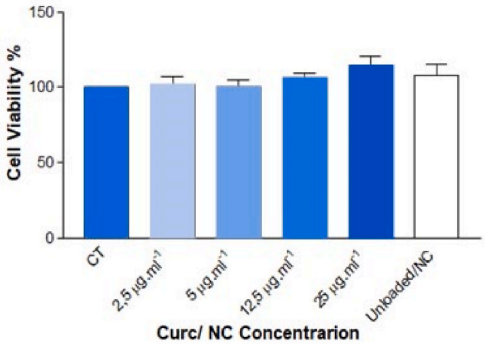


**Fig. 4.** Cytotoxicity study with determination of cell viability) in NIH/3 cell viability T3 murine fibroblasts using resazurin test, where CT = control with DMEM only, and unloaded/NC = 50 % (White) by volume of the formulation without active. Statistical significance was determined by the One-way ANOVA analysis of variance test followed by the Tukey post-test *t*-test for multiple comparisons (*p < 0.05) for n = 3.

polylactic acid derivatives, due to the exposure of highly electronically charged groups. In addition, this surface charge, predominantly negative, helps to prolong the stability of the formulation due to the high repulsion between particles.

LUMiSizer® analysis indicated that stable colloidal dispersions exhibit transmission profiles in a "flat bed" configuration, where the first and last transmission profiles are very close, constant over time, and distributed throughout the sample. The first profiles are represented in red, and the last one in green [55,56]. While less stable particles show a stepped profile due to instability phenomena (sedimentation, flotation, or creaming), resulting in different sedimentation rates and observed differences in the first and last transmission profiles ([55,56]. In Fig. 1A, it can be observed that Curcu/NC has a "flat bed" profile, indicating high stability.

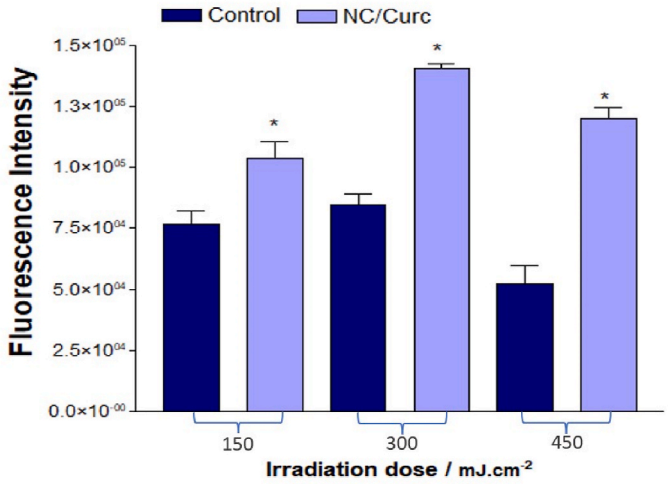


**Fig. 5.** Photobiostimulation assay showing the effect of laser application (150–450 mJ $cm^{-2}$) on the cell viability of human dermal fibroblasts incubated with Curc/NC 5.0 μg $mL^{-1}$ (white); CT = control (black), 48 h after irradiation. The statistical significance of the differences between irradiation doses was determined by the One-way ANOVA analysis of variance test followed by the Tukey *t*-test post-test for multiple comparisons (*$p < 0.05$. Each SEM represents the standard deviation (±SD) for n = 3.

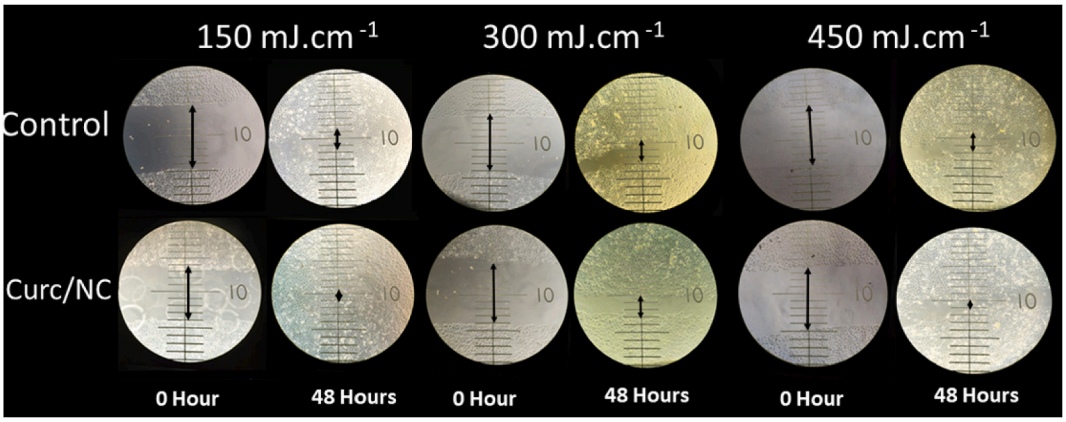


**Fig. 6.** Photomicrographs for monitoring wound closure shortly after irradiation at doses of 150, 300, and 450 mJ $cm^{-2}$, at time 0 and 48 h after irradiation.

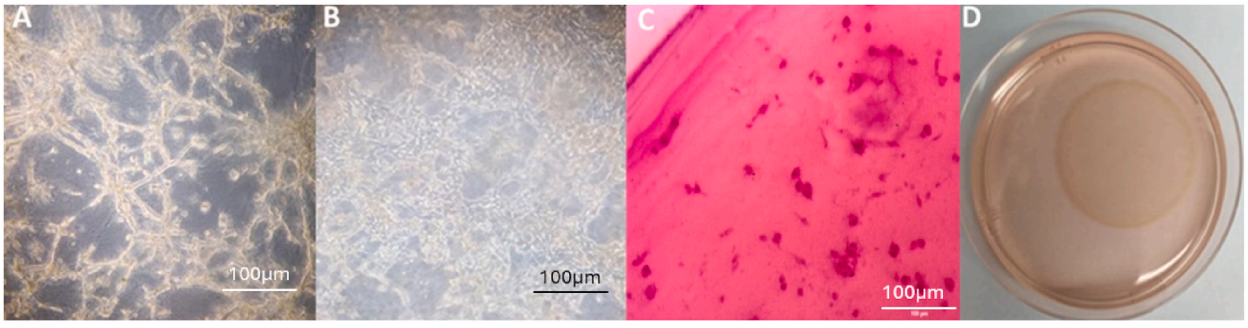


**Fig. 7.** Photomicrographs of (A) Dermic equivalents (B) Three-dimensional skin equivalents (C) TSE stained with hematoxylin and eosin and (D) TSE formed disc.

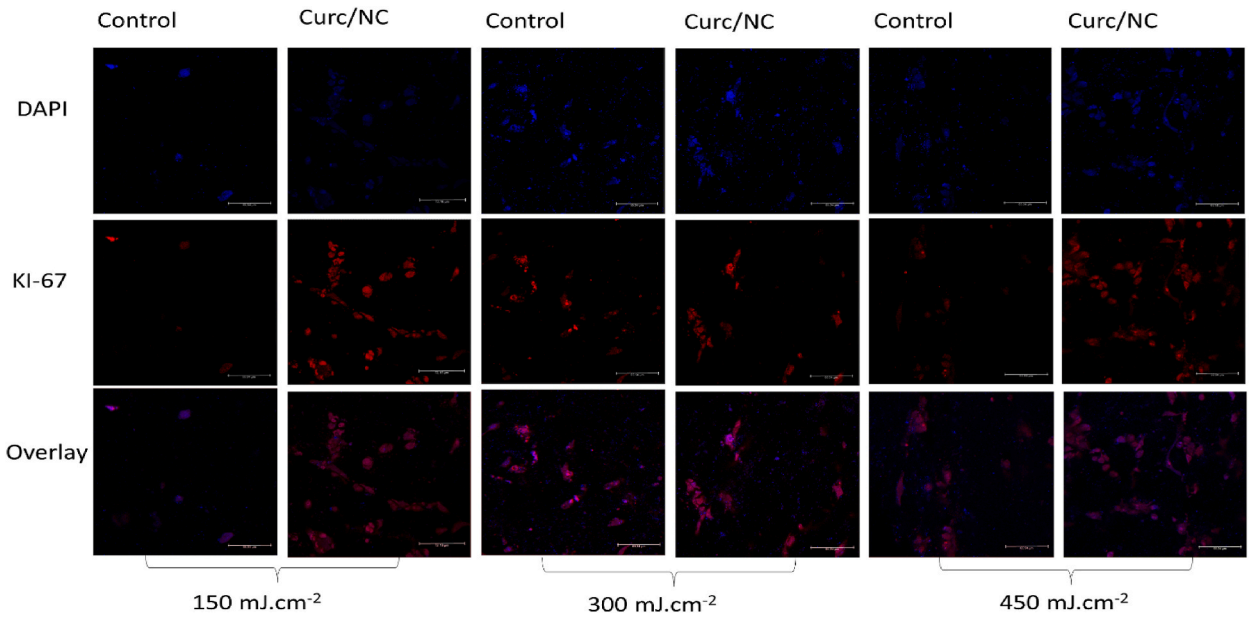


**Fig. 8.** Ki 67 expression in TSEs after incubation with Curc/NC and irradiation with energy doses of 150, 300 and 400 mJ $cm^{-2}$ with their respective controls (without Curc/NC). The image is from the top view of the TSEs.

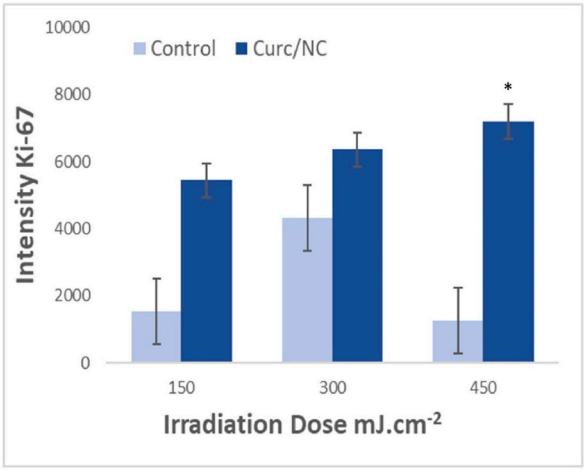


**Fig. 9.** Quantitative data for Ki-67 expression by TSE incubated with Curc/NC and the irradiated controls at 150, 300 and 450 mJ $cm^{-2}$. The statistical significance of the differences between irradiation doses was determined by the One-way ANOVA analysis of variance test followed by the Tukey *t*-test post-test for multiple comparisons (*$p < 0.05$. Each SEM represents the standard deviation (±SD) for $n = 3$.

Additionally, quantitative data in Table 2 show a stability index of approximately 0.042, where a value closer to 0 indicates higher stability, and closer to 1 indicates lower stability. Therefore, it can be concluded that Curc/NC exhibits stability for at least 12 months when stored at 25 °C. On the other hand, NC/undischarged showed differences between the first and last transmission profiles (Fig. 1B), displaying a slightly stepped configuration, which may indicate some instability over time. Quantitative data show an index of approximately 0.240 (Table 2), closer to 0 than 1, indicating a certain level of sample stability.

The cellular uptake of nanomaterials occurs through the endocytosis mechanism (Fig. 3). In the case of NC, where the particles are in a liquid state, this process occurs more specifically through pinocytosis [57,58]. The mechanism of pinocytosis occurs when NC particles approach the cell membrane, this membrane begins a process called invagination where the membrane organizes itself around the particles until it separates from the membrane and forms a vesicle inside the cell [57,59]. The efficiency of cellular uptake is determined by the physical characteristics and interfacial characteristics (NPs) of the nanoparticles. Furthermore, particle size, morphology and surface characteristics such as surface charge and hydrophobicity can also influence absorption pathways. Cell membrane properties and NP interactions with the biological environment also greatly influence cellular uptake [57]. Cellular uptake

of curcumin was significantly improved when performed in NC (Fig. 3), both for the concentrations and incubation times tested, and was used in all cell lines in this study. Previous studies show that curcumin, when associated with a system containing PLGA, has a release time from the first 60 min [60], which indicates that the 3-h incubation time used for in vitro assays is sufficient for curcumin uptake. This can be explained by the submicrometric (nanometric) size of Curc/NCs, as well as their spherical morphology, proven in the MFA assay (Fig. 2A/B), which also favors cellular uptake due to their symmetry and maximum increase in surface area [61]. Furthermore, several studies prove the improvement in the efficiency of therapies using nanostructured curcumin, which in addition to improving its bioavailability, also protects curcumin against its degradation that occurs in an aqueous environment [34,37]. The 3-h incubation time was chosen because it had significant uptake and caused less damage and cellular stress from the assay. After statistical analysis of the cytotoxicity study (Fig. 4) using the One-way ANOVA protocol followed by the Tukey *t*-test post-test, it was observed that there was not any statistical difference between all the samples tested concerning the control. This means there was no significant cell death for any of the samples incubated with different concentrations of the formulation under study after incubation at 3 h. Thus, it can be stated that both Curc/NC and NC/unloaded are very biocompatible with the cellular model used in this test, therefore giving support for subsequent studies of photobiostimulation considering the concentrations of Curc/NC used.

The results of the photobiostimulation assay showed notable cell viability, with values between 135 % and 228 %. These results demonstrate a clear trend towards increased cell proliferation after the application of different doses of irradiation (150, 300 and 450 mJ $cm^{-2}$). Furthermore, the results demonstrate a synpergic effect of PBT and Curc/NC, where they play a significant role in increasing cell proliferation. Curcumin is known for its antioxidant, anti-inflammatory and health-promoting properties. Recent studies have highlighted its potential in regulating cell proliferation, including bone proliferation processes [62]. The monolayer photobiostimulation study using in vitro wound closure monitoring (scratch assay) shows that doses of 300 and 450 mJ.cm-2 (Fig. 6) incubated with Curc/NC present wound closure with reduced times, compared to control. Previous studies show that the association of a PS and laser therapy has an important role in increasing cell migration [63], in addition, as previously mentioned, curcumin has a very important role in cell regeneration [62], with this we can highlight that the synergistic effect between Curc/NC and PBT provided an increase in wound closure kinetics, due to greater cell migration and proliferation.

The objective of obtaining a TSEs (Fig. 7D) was achieved using the already studied DE [45] as a starting point. In Fig. 7B it is possible to observe the formation of the keratinocyte layer on the fibroblast layer in the DE (Fig. 7A), comparing to previous studies with DE where there is no presence of cell co-culture [45,64], we observed that in the model in Fig. 7A there is a beginning of the formation of the epithelial layer characteristic of the skin's natural protection, for example, the basal layer of the epidermal stratum. HE studies (Fig. 7C) showed the presence of cells with different cell morphologies, confirming the formation of TSE by fibroblasts and keratinocytes.

The results of Ki-67 immunohistochemistry show the expression of this marker in all samples, indicating the presence of proliferating cells within the three-dimensional skin models (TSE). Ki-67 is widely recognized as a reliable marker for identifying cells in the active phase of the cell cycle, excluding those at rest (G0 phase), making it a valuable tool for evaluating proliferative activity in different biological contexts. Statistical analysis of the data revealed that only the highest dose of irradiation (450 mJ.cm-2) showed a significant difference in Ki-67 expression between the control group and the group treated with Curc/NC. This result suggests that PBT combined with curcumin in nanocapsules had a more pronounced effect on cell proliferation compared to the control, especially at the higher energy dose. However, we can observe that even at the highest energy dose the statistical difference was significant, there was a tendency for increased proliferation in response to increased irradiation doses, when incubated with Curc/NC. This suggests that even lower doses of irradiation may influence cell proliferation. These results further highlight the synergistic potential of PBT and Curc/NC, in promoting cell proliferation, using a more complex model than monolayer assays, further proving that TSEs can be used as an important tool in the study of efficacy and safety of various therapies related to skin diseases.

Future studies could evaluate the use of curcumin nanocapsules combined with photobiostimulation therapy in in vivo study models, aiming to better understand the synergistic effect of Curc/NC and PBT on tissue regeneration and immune response. Furthermore, its application could be explored in different clinical contexts, in the treatment of skin lesions and inflammatory diseases, and even to promote bone regeneration. However, although this study provides a very important and solid basis, it is necessary to consider that there are limitations, including the need for studies in animal models. This research is essential to ensure the safety and effectiveness of these interventions in the future.

## 5. Conclusion

Based on the results obtained in this research, we can conclude that it is possible to develop a nanostructured polymeric formulation (nanocapsules), containing Curcumin, which shows high physicochemical stability during the 97-day follow-up period. MFA analyses agree with DLS analyses showing particle size <200 nm in addition to spherical morphology with smooth surface and absence of porosity. The cellular internalization assay shows a significant uptake of curcumin when nanostructured compared to its free form. It is possible to observe a better cell uptake with only 3 h of incubation. The monolayer cytotoxicity assay shows cellular biocompatibility with the cell line tested for all concentrations of formulations evaluated, including empty nanocapsules at a rate of 50 % v/v. *In vitro* photobiostimulation studies showed very promising results, demonstrating a potential photobiomodulatory effect of Curc/NC when cellular viability of the HDFn was monitored (>137 % for all LED doses). Concurrently, the methodology for monitoring the closure of lesions and external cells in the HaCaT keratinocyte cell line highlighted that the dose of 300 and 450 mJ $cm^{-2}$ associated with Curc/NC 5.0 μg $mL^{-1}$ showed the most pronounced kinetic effect (proliferative behavior). Three-dimensional skin equivalents were integrated using co-cultures of HdFn and HaCaT. The monitoring by photomicrography proved successful in the formation of multiple cell layers in a tridimensional environment. In addition to it being possible to observe the formation of the keratinocyte layer (HaCaT) on

the upper part of the TSE, the cells stained with hematoxylin and eosin showed two distinct cell morphologies, which evidenced the presence of keratinocytes and fibroblasts in the TSE composition, and consequently the formation of multiple tiers (epidermal basal skin layer). Immunohistochemistry showed Ki-67 expression for all TSE samples, which means the presence of proliferative cells, thus supporting the use of TSE as an excellent in vitro model in the study of various diseases and their potential treatments. Furthermore, Ki-67 expression was much more significant in TSE incubated with Curc/NC, evidencing the biostimulatory potential of curcumin nanocapsules.

## Data availability statement

The data that has been used is confidential.

## CRediT authorship contribution statement

**Camila F. Amantino:** Writing – review & editing, Writing – original draft, Validation, Project administration, Methodology, Investigation, Formal analysis, Data curation, Conceptualization. **Stéphanie R. do Amaral:** Writing – review & editing, Methodology, Investigation. **Mariza Aires-Fernandes:** Writing – review & editing, Funding acquisition. **Sonia M. Oliani:** Resources. **Antonio C. Tedesco:** Resources. **Fernando L. Primo:** Supervision, Resources, Project administration, Conceptualization.

## Declaration of competing interest

The authors declare that they have no known competing financial interests or personal relationships that could have appeared to influence the work reported in this paper.

## Acknowledgments

The authors acknowledge the Brazilian agencies, "Coordenação de Aperfeiçoamento de Pessoal de Nível Superior"—Brazil (CAPES) Finance Code 001, Research Support Foundation of the State of São Paulo (FAPESP, grant no. 2020/09396-8) (grant to M.A.F.), National Concil for Scientif and Technological Development project #310849-2023-3 (grant F.L.P) for the financial support. A.C.T. thanks (FAPESP) Thematic project #2013/50181-1, PRONON-SIPAR project #25000.077093/2015–86, National Council for Scientific and Technological Development (CNPq) grants # 404416/2021-7 (A.C.T.), 441673/2020-1 a 304687/2021-9, and USP-COFECUB Project Agreement #22.1.538.59.4 for their financial support. Dr. Ivana Aparecida Borin at Department of Chemistry of FFCLRP-University of São Paulo at Ribeirão Preto/SP for AFM analysis, Prof. Valéria de Carvalho S. Ebinuma at Department of Bioprocess Engineering and Biotechnology, School of Pharmaceutical Sciences UNESP-Araraquara/SP for EnSpire microplate reader equipment support, and Prof. Dr. Marlus Chorilli at Department of Drugs and Medicines, School of Pharmaceutical Sciences of UNESP-Araraquara/SP for DLS equipment support.

## References

[1] R. Ghafari, M. Jonoobi, L.M. Amirabad, K. Oksman, A.R. Taheri, Fabrication and characterization of novel bilayer scaffold from nanocellulose based aerogel for skin tissue engineering applications, Int. J. Biol. Macromol. 136 (Sep. 2019) 796–803, https://doi.org/10.1016/j.ijbiomac.2019.06.104.
[2] M. Aires-Fernandes, C.F. Amantino, S.R. do Amaral, F.L. Primo, Tissue engineering and photodynamic therapy: a new frontier of science for clinical application -an up-to-date review, Front. Bioeng. Biotechnol. 10 (June) (2022) 1–13, https://doi.org/10.3389/fbioe.2022.837693.
[3] J. Huang, et al., Evaluation of tofu as a potential tissue engineering scaffold, J. Mater. Chem. B 6 (9) (2018) 1328–1334, https://doi.org/10.1039/c7tb02852k.
[4] Q. Zeng, et al., 6.20 Skin tissue engineering, in: Comprehensive Biomaterials II, Elsevier, 2017, pp. 334–382, https://doi.org/10.1016/B978-0-12-803581-8.10157-2.
[5] A. Ganapathy, et al., Guide for starting or optimizing a 3D printing clinical service, Methods 206 (2023) 41–52, https://doi.org/10.1016/j.ymeth.2022.08.003. March 2022.
[6] S.K. Doke, S.C. Dhawale, Alternatives to animal testing: a review, Saudi Pharmaceut. J. 23 (3) (Jul. 01, 2015) 223–229, https://doi.org/10.1016/j.jsps.2013.11.002. Elsevier B.V.
[7] G. Jensen, C. Morrill, Y. Huang, 3D tissue engineering, an emerging technique for pharmaceutical research, Acta Pharm. Sin. B 8 (5) (2018) 756–766, https://doi.org/10.1016/j.apsb.2018.03.006. Chinese Academy of Medical Sciences.
[8] W.C. Yan, et al., 3D bioprinting of skin tissue: from pre-processing to final product evaluation, Adv. Drug Deliv. Rev. 132 (Jul. 01, 2018) 270–295, https://doi.org/10.1016/j.addr.2018.07.016. Elsevier B.V.
[9] Z. Zhang, B.B. Michniak-Kohn, Tissue engineered human skin equivalents, Pharmaceutics 4 (1) (Mar. 2012) 26–41, https://doi.org/10.3390/pharmaceutics4010026.
[10] S. Fink, A. Sethmann, U.C. Hipler, C. Wiegand, In vitro investigation of the principle of action of ammonium bituminosulfonate ointments on a 3D skin model, Eur. J. Pharm. Sci. 172 (February) (2022) 106152, https://doi.org/10.1016/j.ejps.2022.106152.
[11] W. Sun, et al., 3D skin models along with skin-on-a-chip systems: a critical review, Chinese Chem. Lett. 34 (5) (2023) 107819, https://doi.org/10.1016/j.cclet.2022.107819.
[12] M. Nowak-Perlak, P. Ziółkowski, M. Woźniak, A promising natural anthraquinones mediated by photodynamic therapy for anti-cancer therapy, Phytomedicine 119 (2023), https://doi.org/10.1016/j.phymed.2023.155035.
[13] X. Li, et al., Advances in photodynamic therapy of pathologic scar, Photodiagnosis Photodyn. Ther. 46 (December 2023) (2024) 104040, https://doi.org/10.1016/j.pdpdt.2024.104040.
[14] Y. He, L. Luo, L. Liu, Photodynamic therapy for treatment of burns: a system review and meta-analysis of animal study, Photodiagnosis Photodyn. Ther. 45 (November 2023) (2024) 103905, https://doi.org/10.1016/j.pdpdt.2023.103905.
[15] W. Li, et al., In vitro evaluation of ruthenium complexes for photodynamic therapy, Photodiagnosis Photodyn. Ther. 18 (Jun. 2017) 83–94, https://doi.org/10.1016/j.pdpdt.2017.02.001.

[16] Y. Wei, et al., Dicyanomethylene substituted benzothiazole squaraines: the efficiency of photodynamic therapy in vitro and in vivo, EBioMedicine 23 (Sep. 2017) 25–33, https://doi.org/10.1016/j.ebiom.2017.08.010.

[17] L. Benov, Photodynamic therapy: current status and future directions, Med. Princ. Pract. 24 (Apr. 2015) 14–28, https://doi.org/10.1159/000362416.

[18] M. Gendrot, et al., Methylene blue inhibits replication of SARS-CoV-2 in vitro, Int. J. Antimicrob. Agents 56 (6) (2020) 106202, https://doi.org/10.1016/j.ijantimicag.2020.106202.

[19] H. Ma, Y.X. Li, H.L. Chen, M.L. Kang, T.C.Y. Liu, Effects of low-intensity laser irradiation on wound healing in diabetic rats, Int. J. Photoenergy 2012 (2012), https://doi.org/10.1155/2012/838496.

[20] F.H. Li, et al., Photobiomodulation on bax and Bcl-2 proteins and SIRT1/PGC-1 α axis mRNA expression levels of aging rat skeletal muscle, Int. J. Photoenergy 2014 (2014), https://doi.org/10.1155/2014/384816.

[21] P.V. Peplow, T.Y. Chung, G.D. Baxter, Laser photobiomodulation of proliferation of cells in culture: a review of human and animal studies, Photomedicine and Laser Surgery 28 (SUPPL. 1) (2010), https://doi.org/10.1089/pho.2010.2771. Aug. 01.

[22] K.M. AlGhamdi, A. Kumar, N.A. Moussa, Low-level laser therapy: a useful technique for enhancing the proliferation of various cultured cells, Laser Med. Sci. 27 (1) (Jan. 2012) 237–249, https://doi.org/10.1007/s10103-011-0885-2.

[23] N.J. Prindeze, L.T. Moffatt, J.W. Shupp, Mechanisms of action for light therapy: a review of molecular interactions, Exp. Biol. Med. 237 (11) (Nov. 01, 2012) 1241–1248, https://doi.org/10.1258/ebm.2012.012180.

[24] R.D. Novaes, et al., The energy density of laser light differentially modulates the skin morphological reorganization in a murine model of healing by secondary intention, Int. J. Exp. Pathol. 95 (2) (Apr. 2014) 138–146, https://doi.org/10.1111/iep.12063.

[25] N. Elson, D. Foran, Low level laser therapy in modern dentistry, Periodontics Prosthodont. 1 (1) (2015), https://doi.org/10.21767/2471-3082.100002.

[26] P. Deyhimi, H. Khademi, R. Birang, M. Akhoondzadeh, C. Author, Histological Evaluation of Wound Healing Process after Photodynamic Therapy of Rat Oral Mucosal Ulcer, 2016.

[27] M.P. Siqueira-Moura, F.L. Primo, E.M. Espreafico, A.C. Tedesco, Development, characterization, and photocytotoxicity assessment on human melanoma of chloroaluminum phthalocyanine nanocapsules, Mater. Sci. Eng. C 33 (3) (2013) 1744–1752, https://doi.org/10.1016/j.msec.2012.12.088. Apr.

[28] A. Tedesco, P. Jesus, Low level energy photodynamic therapy for skin processes and regeneration, in: Photomedicine - Advances in Clinical Practice, InTech, 2017, https://doi.org/10.5772/65344.

[29] R. Fekrazad, S. Asefi, K. Khorsandi, M. Nejatifard, Photo biostimulatory effect of low dose photodynamic therapy on human mesenchymal stem cells, Photodiagnosis Photodyn. Ther. 31 (Sep) (2020), https://doi.org/10.1016/j.pdpdt.2020.101886.

[30] S. Kwiatkowski, et al., Photodynamic therapy – mechanisms, photosensitizers and combinations, Biomed. Pharmacother. 106 (Oct. 01, 2018) 1098–1107, https://doi.org/10.1016/j.biopha.2018.07.049. Elsevier Masson SAS.

[31] F.C. Machado, R.P. Adum de Matos, F.L. Primo, A.C. Tedesco, P. Rahal, M.F. Calmon, Effect of curcumin-nanoemulsion associated with photodynamic therapy in breast adenocarcinoma cell line, Bioorganic Med. Chem. 27 (9) (2019) 1882–1890, https://doi.org/10.1016/j.bmc.2019.03.044.

[32] R.P.A. De Matos, et al., Effect of curcumin-nanoemulsion associated with photodynamic therapy in cervical carcinoma cell lines, BioMed Res. Int. 2018 (2018), https://doi.org/10.1155/2018/4057959.

[33] F. Guan, Y. Ding, Y. Zhang, Y. Zhou, M. Li, C. Wang, Curcumin suppresses proliferation and migration of MDA-MB-231 breast cancer cells through autophagy-dependent Akt degradation, PLoS One 11 (1) (Jan. 2016), https://doi.org/10.1371/journal.pone.0146553.

[34] K. Gayathri, M. Bhaskaran, C. Selvam, R. Thilagavathi, Nano formulation approaches for curcumin delivery- a review, J. Drug Deliv. Sci. Technol. 82 (March) (2023) 104326, https://doi.org/10.1016/j.jddst.2023.104326.

[35] F. da S. Feltrin, T. Agner, C. Sayer, L.M.F. Lona, Curcumin encapsulation in functional PLGA nanoparticles: a promising strategy for cancer therapies, Adv. Colloid Interface Sci. 300 (2022) 102582, https://doi.org/10.1016/j.cis.2021.102582.

[36] M. Hasan, et al., Liposome encapsulation of curcumin: physico-chemical characterizations and effects on MCF7 cancer cell proliferation, Int. J. Pharm. 461 (1–2) (2014) 519–528, https://doi.org/10.1016/j.ijpharm.2013.12.007.

[37] M. Moniruzzaman, T. Min, Curcumin, curcumin nanoparticles and curcumin nanospheres: a review on their pharmacodynamics based on monogastric farm animal, poultry and fish nutrition, Pharmaceutics 12 (5) (2020), https://doi.org/10.3390/pharmaceutics12050447.

[38] G. Birhanu, H.A. Javar, E. Seyedjafari, A. Zandi-Karimi, Nanotechnology for delivery of gemcitabine to treat pancreatic cancer, Biomed. Pharmacother. 88 (2017) 635–643, https://doi.org/10.1016/j.biopha.2017.01.071. Elsevier Masson SAS.

[39] Z. Zhang, et al., Evaluation of photodynamic therapy using topical aminolevulinic acid hydrochloride in the treatment of condylomata acuminate, Int. J. Clin. Exp. Med. 8 (4) (2015) 6517–6521.

[40] D.C. Zancanela, F.L. Primo, A.L. Rosa, P. Ciancaglini, A.C. Tedesco, The effect of photosensitizer drugs and light stimulation on osteoblast growth, Photomed. Laser Surg 29 (10) (Oct. 2011) 699–705, https://doi.org/10.1089/pho.2010.2929.

[41] C.F. Amantino, Á. de Baptista-Neto, A.C. Badino, M.P. Siqueira-Moura, A.C. Tedesco, F.L. Primo, Anthraquinone encapsulation into polymeric nanocapsules as a new drug from biotechnological origin designed for photodynamic therapy, Photodiagnosis Photodyn. Ther. 31 (Sep) (2020), https://doi.org/10.1016/j.pdpdt.2020.101815.

[42] B.R. Davey, What Are Nanocapsules ? Nanocapsules – an Overview Delivering Drugs Using Nanocapsules Derived from Cow ' S Milk, 2021, pp. 1–5.

[43] H. Fessi, F. Puisieux, J.P. Devissaguet, N. Ammoury, S. Benita, Nanocapsule formation by interfacial polymer deposition following solvent displacement, Int. J. Pharm. 55 (1) (1989) 1–4, https://doi.org/10.1016/0378-5173(89)90281-0.

[44] A.D. Premarathna, et al., Wound healing properties of aqueous extracts of Sargassum illicifolium: an in vitro assay, Wound Med 24 (1) (2019) 1–7, https://doi.org/10.1016/j.wndm.2018.11.001.

[45] F.L. Primo, L.B. De Paula, M.P. De Siqueira-Moura, A.C. Tedesco, "Photobiostimulation on Wound Healing Treatment by ClAlPc-nanoemulsion from a Multiple-Wavelength Portable Light Source on a 3D-Human Stem Cell Dermal Equivalen," 19 (2012) 5157.

[46] Y.Y. Kim, et al., Laminin peptide YIGSR enhances epidermal development of skin equivalents, J. Tissue Viability 27 (2) (May 2018) 117–121, https://doi.org/10.1016/j.jtv.2018.02.001.

[47] A. Zielińska, C. Martins-Gomes, N.R. Ferreira, A.M. Silva, I. Nowak, E.B. Souto, Anti-inflammatory and anti-cancer activity of citral: optimization of citral-loaded solid lipid nanoparticles (SLN) using experimental factorial design and LUMiSizer, Int. J. Pharm. 553 (1–2) (2018) 428–440, https://doi.org/10.1016/j.ijpharm.2018.10.065.

[48] A.R. Fernandes, et al., Ibuprofen nanocrystals developed by 22 factorial design experiment: a new approach for poorly water-soluble drugs, Saudi Pharm. J. 25 (8) (2017) 1117–1124, https://doi.org/10.1016/j.jsps.2017.07.004.

[49] H. Bi, Y. Jin, Current progress of skin tissue engineering: seed cells, bioscaffolds, and construction strategies, Burn. Trauma 1 (2) (2013) 63–72, https://doi.org/10.4103/2321-3868.118928.

[50] D. Lv, Z. Hu, L. Lu, H. Lu, X. Xu, Three-dimensional cell culture: a powerful tool in tumor research and drug discovery, Oncol. Lett. 14 (6) (2017) 6999–7010, https://doi.org/10.3892/ol.2017.7134.

[51] M. Pal, et al., Epithelial-mesenchymal transition of cancer cells using bioengineered hybrid scaffold composed of hydrogel/3D-fibrous framework, Sci. Rep. 9 (1) (2019) 1–11, https://doi.org/10.1038/s41598-019-45384-9.

[52] L. Treuel, S. Brandholt, P. Maffre, S. Wiegele, L. Shang, G.U. Nienhaus, Impact of protein modification on the protein corona on nanoparticles and nanoparticle-cell interactions, ACS Nano 8 (1) (Jan. 2014) 503–513, https://doi.org/10.1021/nn405019v.

[53] S. Bhattacharjee, DLS and zeta potential - what they are and what they are not? J. Contr. Release 235 (Aug. 10, 2016) 337–351, https://doi.org/10.1016/j.jconrel.2016.06.017. Elsevier B.V.

[54] P.P. dos Santos, S.H. Flôres, A. de Oliveira Rios, R.C. Chisté, Biodegradable polymers as wall materials to the synthesis of bioactive compound nanocapsules, Trends Food Sci. Technol. 53 (Jul. 01, 2016) 23–33, https://doi.org/10.1016/j.tifs.2016.05.005. Elsevier Ltd.

[55] C. Caddeo, et al., Nanocarriers for antioxidant resveratrol: formulation approach, vesicle self-assembly and stability evaluation, Colloids Surfaces B Biointerfaces 111 (2013) 327–332, https://doi.org/10.1016/j.colsurfb.2013.06.016.

[56] I. Pereira, A. Zielińska, N.R. Ferreira, A.M. Silva, E.B. Souto, Optimization of linalool-loaded solid lipid nanoparticles using experimental factorial design and long-term stability studies with a new centrifugal sedimentation method, Int. J. Pharm. 549 (1–2) (2018) 261–270, https://doi.org/10.1016/j.ijpharm.2018.07.068.
[57] I.M. Adjei, B. Sharma, V. Labhasetwar, Nanoparticles: cellular uptake and cytotoxicity, Adv. Exp. Med. Biol. 811 (2014) 73–91, https://doi.org/10.1007/978-94-017-8739-0_5.
[58] C. Souza, C.C. Jayme, N. Rezende, A.C. Tedesco, Synergistic effect of photobiomodulation and phthalocyanine photosensitizer on fibroblast signaling responses in an in vitro three-dimensional microenvironment, J. Photochem. Photobiol. B Biol. 222 (Sep) (2021), https://doi.org/10.1016/j.jphotobiol.2021.112256.
[59] M. Bohdanowicz, S. Grinstein, Role of phospholipids in endocytosis, phagocytosis, and macropinocytosis, Physiol. Rev. 93 (1) (2013) 69–106, https://doi.org/10.1152/physrev.00002.2012.
[60] M. Chen, et al., The kinetics and release behaviour of curcumin loaded pH-responsive PLGA/chitosan fibers with antitumor activity against HT-29 cells, Carbohydr. Polym. 265 (January) (2021) 118077, https://doi.org/10.1016/j.carbpol.2021.118077.
[61] M.L. Del Prado-Audelo, et al., In vitro cell uptake evaluation of curcumin-loaded PCL/F68 nanoparticles for potential application in neuronal diseases, J. Drug Deliv. Sci. Technol. 52 (March) (2019) 905–914, https://doi.org/10.1016/j.jddst.2019.05.042.
[62] J. Wei, et al., Switch-on mode of bioenergetic channels regulated by curcumin-loaded 3D composite scaffold to steer bone regeneration, Chem. Eng. J. 452 (P1) (2023) 139165, https://doi.org/10.1016/j.cej.2022.139165.
[63] R. Yang, S. Guo, S. Xiao, Y. Ding, Enhanced wound healing and osteogenic potential of photodynamic therapy on human gingival fibroblasts, Photodiagnosis Photodyn. Ther. 32 (August) (2020) 101967, https://doi.org/10.1016/j.pdpdt.2020.101967.
[64] F.L. Primo, M.B. Da Costa Reis, M.A. Porcionatto, A.C. Tedesco, "In Vitro Evaluation of Chloroaluminum Phthalocyanine Nanoemulsion and Low-Level Laser Therapy on Human Skin Dermal Equivalents and Bone Marrow Mesen-chymal Stem Cells," v. 18, n. 22, p. 3376–3381 (2011).